Characterization of Immune Cell Populations of Cutaneous Neurofibromas in Neurofibromatosis 1

Kallionpää, Roope A; Peltonen, Sirkku; Le, Kim My; Martikkala, Eija; Jääskeläinen, Mira; Fazeli, Elnaz; Riihilä, Pilvi; Haapaniemi, Pekka; Rokka, Anne; Salmi, Marko; Leivo, Ilmo; Peltonen, Juha

Published in:
Laboratory Investigation

DOI:
10.1016/j.labinv.2023.100285

Published: 01/01/2024

Document Version
Final published version

Document License
CC BY-NC-ND

Lab Invest 104 (2024) 100285

LABORATORY INVESTIGATION

journal homepage: https://laboratoryinvestigation.org/

Research Article

Characterization of Immune Cell Populations of Cutaneous Neurofibromas in Neurofibromatosis 1

Roope A. Kallionpää[a,b], Sirkku Peltonen[c,d,e,f,g,h], Kim My Le[a], Eija Martikkala[a], Mira Jääskeläinen[a], Elnaz Fazeli[a,i], Pilvi Riihilä[c,d,j], Pekka Haapaniemi[k], Anne Rokka[k], Marko Salmi[a,l], Ilmo Leivo[a], Juha Peltonen[a,b,*]

[a] *Institute of Biomedicine, University of Turku, Turku, Finland;* [b] *FICAN West Cancer Centre, University of Turku and Turku University Hospital, Turku, Finland;* [c] *Department of Dermatology and Venereology, University of Turku, Turku, Finland;* [d] *Department of Dermatology, Turku University Hospital, Turku, Finland;* [e] *Department of Dermatology and Venereology, Institute of Clinical Sciences, Sahlgrenska Academy, University of Gothenburg, Gothenburg, Sweden;* [f] *Department of Dermatology and Venereology, Region Västra Götaland, Sahlgrenska University Hospital, Gothenburg, Sweden;* [g] *Department of Dermatology and Allergology, University of Helsinki, Helsinki, Finland;* [h] *Skin and Allergy Hospital, Helsinki University Hospital, Helsinki, Finland;* [i] *Biomedicum Imaging Unit, Faculty of Medicine and HiLIFE, University of Helsinki, Helsinki, Finland;* [j] *FICAN West Cancer Research Laboratory, University of Turku and Turku University Hospital, Turku, Finland;* [k] *Turku Bioscience Centre, University of Turku and Åbo Akademi University, Turku, Finland;* [l] *MediCity Research Laboratory, and InFLAMES Research Flagship Center, University of Turku, Turku, Finland*

ARTICLE INFO

Article history:
Received 30 May 2023
Revised 20 October 2023
Accepted 3 November 2023
Available online 8 November 2023

Keywords:
benign tumor
immune system
macrophage
mass spectrometry
neurofibroma
skin
T cell receptor
T lymphocyte
tumor microenvironment

ABSTRACT

Cutaneous neurofibromas (cNFs) are characteristic of neurofibromatosis 1 (NF1), yet their immune microenvironment is incompletely known. A total of 61 cNFs from 10 patients with NF1 were immunolabeled for different types of T cells and macrophages, and the cell densities were correlated with clinical characteristics. Eight cNFs and their overlying skin were analyzed for T cell receptor CDR domain sequences, and mass spectrometry of 15 cNFs and the overlying skin was performed to study immune-related processes. Intratumoral T cells were detected in all cNFs. Tumors from individuals younger than the median age of the study participants (33 years), growing tumors, and tumors smaller than the data set median showed increased T cell density. Most samples displayed intratumoral or peritumoral aggregations of CD3-positive cells. T cell receptor sequencing demonstrated that the skin and cNFs host distinct T cell populations, whereas no dominant cNF-specific T cell clones were detected. Unique T cell clones were fewer in cNFs than in skin, and mass spectrometry suggested lower expression of proteins related to T cell-mediated immunity in cNFs than in skin. CD163-positive cells, suggestive of M2 macrophages, were abundant in cNFs. Human cNFs have substantial T cell and macrophage populations that may be tumor-specific.

Introduction

Multiple cutaneous neurofibromas (cNFs) are a hallmark of neurofibromatosis type 1 (NF1). These tumors typically start to appear in puberty, and their number increases with age.[1] Although cNFs are invariably benign and rarely exceed the size of a few centimeters, their number may exceed hundreds or thousands,[2,3] and the tumors markedly decrease the quality of life of the affected individuals.[4,5] NF1 is caused by pathogenic variants of the tumor-suppressor gene *NF1*,[6,7] and it has a prevalence of 1/3000 to 1/2000.[8] NF1 is a tumor predisposition syndrome with an

* Corresponding author.
E-mail address: juhpel@utu.fi (J. Peltonen).

https://doi.org/10.1016/j.labinv.2023.100285

increased risk for malignant tumors of the central and peripheral nervous systems, breast, and gastrointestinal tract.[9]

Plexiform neurofibroma is another benign tumor type typical for NF1, but in contrast to cNFs, plexiform neurofibromas can undergo transformation into malignant peripheral nerve sheath tumors.[10] Both cutaneous and plexiform neurofibromas are considered to originate from a subpopulation of Schwann cell precursors with a somatic "second-hit" *NF1* mutation.[11-13] In addition to Schwann cells, neurofibromas contain a mixed population of other cell types of peripheral nerve.[14,15] Of immune cells, mast cells have long been known to be abundant in neurofibromas, and we have recently shown that the subtypes of mast cells in cNFs are distinct from those seen in unaffected skin.[16]

The studies on tumor immunity have focused almost entirely on malignant tumors, whereas the role of the immune system in benign tumors has received very little attention.[17] Immunity plays a central and complex role in propagating or inhibiting tumor growth. Solid malignant tumors contain immune cells that interact with the surrounding microenvironment, and the characterization of tumor-infiltrating lymphocytes has been a crucial step in the successful development of immunotherapies.[18] Studies on melanocytic nevi have shown that the numbers of infiltrating lymphocytes are increased in the transition from benign melanocytic nevus to malignant melanoma.[19] Benign melanocytic nevi harbor dominantly $CD4^+$ inflammatory cells, whereas the relative number of cytotoxic $CD8^+$ cells is increased in regressing nevi.[20] The numbers of CD25 and FoxP3 expressing regulatory T cells are increased in atypical nevi, suggesting that they induce immunotolerance early during malignant transformation to melanoma.[20]

Our knowledge of neurofibroma tumor immune microenvironment is largely derived from animal models of plexiform neurofibromas.[21,22] An *Nf1* haploinsufficient bone marrow fosters the development of murine plexiform neurofibromas[23] and increases the immune infiltration into plexiform tumors.[24] Previous studies have demonstrated abundant macrophages in mouse plexiform neurofibromas.[21,25,26] T cells have received little attention in the context of NF1, yet data from mouse models have suggested that T cells have an essential role in maintaining the macrophage population of plexiform neurofibromas.[27] T cells, positive for CD8, are also known to contribute to the growth of *Nf1*-associated low-grade glioma in a murine model.[28] Brosseau and coworkers suggested that despite the predisposition to benign tumors, *Nf1* haploinsufficient tumor microenvironment may act against malignant degeneration via a T cell-mediated mechanism.[29]

Human cNFs and their Schwann cells express programmed death ligand 1 (PD-L1),[30,31] and malignant peripheral nerve sheath tumors are associated with increased expression of PD-L1 compared with benign tumors,[32,33] which highlights the relevance of the immune system in NF1-associated tumors. Farschtschi and coworkers[34] have examined the counts of circulating lymphocytes in patients with NF1 and show generalized lymphopenia. The fractions of $CD8^+CD27^-$ and $CD8^+CD57^+$ effector T cells were increased in NF1 patients with low internal tumor load and were decreased to levels below controls in patients with high tumor load.[34] Single-cell sequencing of cNFs suggested that all tumors had a population of resting $CD4^+$ memory T cells, in addition to activated mast cells and M2 macrophages.[35] Moreover, immunohistochemistry of cNFs has shown the presence of cells positive for CD3, CD4, CD8, CD68, and FoxP3.[30,31] However, the T cell population of human cNFs has not been previously investigated in quantitative detail, even though the characterization and quantification of different cell types in cNFs have been identified as a key to developing better therapies.[36]

T cell receptor (TCR) can be used to characterize T cell populations present in tissues (for review see Frank et al[37]). TCRs recognize protein epitopes displayed by antigen-presenting cells. These receptors play an essential role in regulating the selection, function, and activation of T cells, and they also allow the identification of a single cell's clonal ancestry or clonotype.

This study was initiated to increase understanding of the development and characteristics of cNFs and to elucidate potential therapeutic targets in the T cell immunity for cNFs. We have immunolabeled 61 cNFs from 10 patients using markers for T cells and macrophages. Intratumoral T cells were further characterized by TCR sequencing, and immunologic processes were surveyed using mass spectrometry. The study is thus designed to provide an overview of the immune cell microenvironment in cNFs.

Materials and Methods

The study is based on cNF samples from patients visiting the NF1 clinic operative in Turku University Hospital, Turku, Finland. All sample donors fulfilled the National Institutes of Health diagnostic criteria for NF1.[38,39] The cNFs were excised using a CO_2 laser on the patient's initiative, typically because of itching, pain, growth, abrasion, or visual obtrusiveness. The study adhered to the principles of the Declaration of Helsinki and was approved by the Ethics Committee of the Hospital District of Southwest Finland and Turku University Hospital. All participants provided their written informed consent.

Immunohistochemistry

A total of 61 formalin-fixed cNFs from 5 men and 5 women with a median age of 33 years (24-52 years), stored in 32 paraffin blocks, were immunolabeled for T cell and macrophage markers. The CD3, CD4, and CD8 immunolabeling was performed using the Ventana Benchmark Ultra system (Roche) in the accredited Pathology Laboratory of Turku University Hospital. The samples, fixed in 10% neutral formalin immediately after excision, were cut into 3-μm sections. Primary antibodies were preceded by antigen retrieval with Cell Conditioning Solution CC1 (Roche) for 64 minutes in the CD3 and CD4 immunolabeling and 52 minutes in the CD8 immunolabeling. Details of the primary antibodies are shown in Supplementary Table S1. The primary antibodies were incubated for 32 minutes. The labeling was detected with 3,3'-diaminobenzidine (DAB) as a chromogen (ultraView Universal DAB Detection Kit, Roche, for CD3 and CD8; OptiView DAB IHC Detection Kit, Roche, for CD4). All sections were counterstained with hematoxylin.

The samples were immunolabeled for FoxP3, CD68, and CD163 in the Histology core facility of the Institute of Biomedicine, University of Turku. Microwave antigen retrieval was performed twice for 7 minutes in Dako Target Retrieval Solution (Agilent), in pH 9 for FoxP3 and CD163 and pH 6 for CD68. After pretreatment with 3% hydrogen peroxide to block endogenous peroxidase activity, the samples were incubated with the primary antibodies (Supplementary Table S1) diluted in Dako Antibody Diluent solution (Agilent) for 1 hour. The primary antibodies were followed by BrightVision+ postantibody blocking solution (ImmunoLogic) for 20 minutes, BrightVision+ Anti-IgG poly-HRP (ImmunoLogic) for 30 minutes, and detection with DAB as a chromogen using Dako DAB+ Substrate Chromogen System (Agilent) for 10 minutes. The slides were counterstained with hematoxylin.

A subset of samples was immunolabeled for S100 using the Benchmark Ultra system (Roche) to detect cNF Schwann cells. The samples were pretreated with Cell Conditioning Solution CC1 (Roche) for 52 minutes and incubated with the anti-S100 primary antibody (Supplementary Table S1) for 32 minutes. The ultraView Universal DAB Detection Kit (Roche) was used for detection.

The immunohistochemical slides were digitized using the Pannoramic 250 and Pannoramic Midi FL slide scanners (3DHistech Ltd).

Immunofluorescence Labeling

For the further characterization of the immune microenvironment in cNFs, 12 fresh-frozen tumors from 6 patients were labeled for interleukin-25 (IL-25), 5 formalin-fixed, paraffin-embedded tumors from 5 patients were labeled for cytotoxic T-lymphocyte-associated protein 4 (CTLA4), and 8 fresh-frozen tumors from 5 patients were double-labeled for FoxP3 and CD25.

Indirect immunofluorescence labeling with monoclonal antibody to IL-25 (Supplementary Table S1) was carried out overnight at 4 °C on acetone-fixed frozen sections following a previously described protocol.[40] Goat anti-mouse IgG (H+L) conjugated to Alexa Fluor 488 (A-11029) diluted 1:500 was used for detection, and Hoechst 33342 diluted 1:10,000 was used for the visualization of nuclei (both reagents from Thermo Fisher Scientific), and the samples were incubated for 1.5 hours at room temperature.

Labeling for CTLA4 was preceded by 2 × 5 minutes of microwave-assisted antigen retrieval at pH 9. The labeling was carried out on formalin-fixed, paraffin-embedded tissue sections using a polyclonal anti-CTLA4 antibody (Supplementary Table S1) overnight at 4 °C.[40] Goat anti-rabbit IgG (H+L) linked with Alexa Fluor 568 (A-11011; Thermo Fisher Scientific) diluted at a ratio of 1:1000 was used as the secondary antibody, and the nuclei were detected with Hoechst 33342 diluted 1:10,000. The secondary antibody was incubated with the samples for 1.5 hours at room temperature.

For FoxP3 and CD25 double labeling, frozen sections were fixed with ice-cold acetone and first incubated with anti-FoxP3 antibody (Supplementary Table S1) overnight at 4 °C, and goat anti-rabbit IgG (H+L) linked with Alexa Fluor 568 (A-11011) diluted 1:1000 for 1.5 hours at room temperature. The sections were then fixed with 10% neutral formalin for 10 minutes and incubated with monoclonal antibody for CD25 (Supplementary Table S1) overnight at 4 °C. Goat anti-mouse IgG (H+L) linked with Alexa Fluor 488 (A-11029) diluted 1:500, and Hoechst 33342 diluted 1:10,000 were used for detection with incubation for 1.5 hours at room temperature.

Immunofluorescence labeling was imaged using a Zeiss AxioImager M1 microscope (Carl Zeiss AG).

Quantification of Cells Positive for CD3, CD4, CD8, or FoxP3

QuPath software version 0.1.2[41] was used to quantify positively labeled cells in digitized slides. The tumor area was manually annotated to separate the tumor from the surrounding dermis. Artifacts, such as ruptures and damaged border areas, were excluded.

Each slide labeled for CD3, CD4, CD8, and FoxP3 was independently scored by 2 raters (R.A.K. and E.M.) for the overall uneven spatial distribution of positive cells, peritumoral clustering of positive cells, and intratumoral clustering of positive cells. The raters discussed the assessment criteria with examples of different patterns of positive cell distribution before commencing the scoring task. Each variable was considered positive if at least one rater reported cell clustering of interest. The percent agreement between the 2 raters was 77% to 88% for the different markers in the case of uneven distribution, 76% to 87% in the case of peritumoral clustering, and 72% to 93% in the case of intratumoral clustering.

Cells positive for CD3, CD8, or FoxP3 and the total number of cells within the annotated tumor area were counted using the positive cell detection functionality of the QuPath software application. Optical density sum was used as the detection image. The counts of positive cells were divided by the annotated tumor area to obtain positive cell density as cells/mm^2. Tumor cellularity was computed as the ratio of the total number of cells and tumor area, and the average of the values determined from CD3, CD8, and FoxP3 immunolabeled sections was used in the analyses. Similarly, the average tumor area in the different sections was used as a surrogate for tumor size. Although the tumor area of the formalin-fixed sections does not correspond to the original size of the tumor, the area serves as a measure of relative tumor size within the data set.

The spatial distribution patterns of positive cells and log-transformed positive cell densities were compared with respect to tumor size, cellularity, and various clinical characteristics. The clinical characteristics were recorded by the physician performing the tumor excision (S.P. and P.R.) and included sex, age at tumor excision, tumor location (trunk vs other), the presumed growth status of the tumor (growing vs no evidence of recent growth; estimated by an experienced clinician based on the patient's report), and the estimated total cNF number of the individual ($\leq$500 vs >500). For age, cellularity, and tumor size, cNFs below the data set median were compared with those above the data set median. In addition to the plain positive cell densities, the ratio of the densities of CD3- and CD8-positive cells was studied. Linear mixed-effects regression was used for the comparisons of positive cell densities, and generalized linear mixed-effects regression with binomial distribution was used for analyzing the spatial distribution patterns. A random intercept for each patient was included to account for the correlation of tumor features within individuals. The R software for statistical computing (version 4.0.0) was used for the statistical analyses.

Quantification of Cells Positive for CD68 or CD163

Due to the relatively irregular shape of the cells positive for CD68 or CD163, automated cell counting was not possible. The annotated tumor area was divided into tiles of 1 × 1 mm, and 5 tiles per tumor were randomly chosen for manual cell counting. The number of positive cells in these tiles was divided by the area of the tiles to obtain the average density of positive cells in the tumor. The statistical comparisons of the densities of cells positive for CD68 or CD163 with respect to clinical characteristics and tumor properties were performed analogously to those of cells positive for CD3, CD8, and FoxP3. In addition, the densities of cells positive for CD68 or CD163 were correlated with the density of cells positive for CD3 and the previously reported density of cells positive for the mast cell marker CD117[16] using linear mixed-effects regression with a random intercept for each patient.

Mass Spectrometry

The protein levels in cNFs and the overlying skin were compared using a mass spectrometry (MS) data set reported elsewhere

(Kallionpää et al, unpublished data). Data from matched cNF and skin samples were available from 15 tumors from 1 male and 3 females with NF1. The data were based on peptides isolated from fresh-frozen tumors using pressure-based lysis and trypsin digestion, followed by liquid chromatography-electrospray ionization-MS/MS (Kallionpää et al, unpublished data). The data contained imputed values for proteins whose absence was likely due to low expression levels in either tissue type (Kallionpää et al, unpublished data). The data set covered 2461 proteins, 99.96% of which were detected in both cNF and skin. Each protein was linked to the associated gene ontology (GO) terms (release 2021-07-02) using the UniProt identifier as a key.[42,43]

The log-transformed normalized protein levels associated with immune-related GO terms were compared between cNFs and skin using linear mixed-effects regression models allowing for a random intercept for each protein and nested random intercepts for each patient and sample. Only GO terms with data from more than 4 proteins were analyzed. In the case of model nonconvergence, the random intercept for each patient was first omitted, and if necessary, the random intercept for each sample was then removed from the model. Bonferroni correction was applied to the *P* values. A small set of proteins (STAT6, CD14, CD39, CD73, and CD163) was also analyzed at the protein level following the same protocol but without a random intercept for each protein. The analyses were performed using R software for statistical computing, version 4.0.0.

T Cell Receptor Sequencing

For TCR sequencing, 9 cNFs from 3 patients with NF1 were collected. The skin overlying the tumor was separated immediately after tumor removal. Venous blood sample was taken at the same patient visit. Genomic DNA was freshly isolated from tumor and skin samples using phenol-chloroform isoamyl alcohol extraction and from blood using Illustra Nucleon BACC3 kit (Cytiva). The DNA was quantified using a QIAxpert spectrophotometer. One cNF sample yielded insufficient DNA for further analysis. The DNA samples were diluted to 30 ng/μL and sent to Adaptive Biotechnologies where the sequencing of the CDR3 region of TCR was carried out. The somatically rearranged human CDR3 was amplified from genomic DNA using a two-step, amplification bias-controlled multiplex PCR approach.[44,45] The first PCR consisted of forward and reverse amplification primers specific for every known V and J gene segment and amplified the hypervariable CDR3 of the immune receptor locus. The method amplified only recombined TCR genes because of a large intron between V and J genes.[44] The second PCR added a proprietary barcode sequence and Illumina adapter sequences.[46] In addition, reference gene primers were included in the PCR reaction to quantify total sequencable nucleated cells and accurately measure the fraction of T cells in each sample. CDR3 and reference gene libraries were sequenced on an Illumina instrument according to the manufacturer's instructions.

The immunoSEQ analyzer tool (Adaptive Biotechnologies) was used to compute the numbers of TCR rearrangements and templates, the fraction of productive templates, ie, templates that can produce a functional protein receptor, maximum productive frequency, and productive Simpson clonality for each sample. Productive Simpson clonality was calculated as the square root of Simpson's diversity index for all productive rearrangements.[47] The values of productive Simpson clonality can range from 0 to 1, with 1 indicating the predominance of one or a few clones. These metrics were summarized over samples as means and standard deviations (SD) and compared between different tissues using linear mixed-effects regression with a random intercept for each patient. The numbers of rearrangements were log-transformed, and Simpson clonality values were square-transformed to ensure the normality of residuals. In addition, Morisita's overlap index was used to study the overlap of rearrangements between pairs of samples.[48] Morisita index values near 0 indicate little overlap between samples, and values near 1 indicate high overlap. The mean Morisita index values between pairs of certain tissues were compared using two-sided *t* tests.

To further examine the overlap of productive rearrangements between different samples, rearrangements present in the blood of a patient were excluded from the respective cNF and skin samples. Circulating T cells or tissue cross-contamination during surgical operation could cause the detection of blood T cells not present in the tissue and therefore lead to artificially extensive overlaps between the tissue types. The results were visualized using Venn diagrams. For statistical analysis and visualization, we used the R software for statistical computing, version 4.0.0, and packages lmerTest, version 3.1-2, and gplots, version 3.1.3.

Results

Immunolabeling of T Cell Populations in Cutaneous Neurofibromas

A total of 61 cNFs from 10 individuals with NF1 (3-16 cNFs per individual) were immunolabeled (Table 1). The majority of the cNFs displayed uneven spatial distribution of cells positive for the T cell markers (Table 1). The immunolabeling patterns suggested the presence of the following 3, partly overlapping categories of T cell distribution (Fig. 1; Table 1): (1) mostly uniform scattering of T cells throughout the tumor (14.8% of cNFs immunolabeled for CD3), (2) clustering of immune cells inside the tumor (61.1% of cNFs), and (3) clustering of immune cells at tumor border (68.5% of cNFs). Even in tumors with clear clustering of T cells at the tumor border, or deeper inside the tumor, there were also scattered individual cells positive for the T cell markers throughout the tumor mass. The percentages of samples exhibiting each pattern varied

Table 1
The quantification results of immunolabeling for various markers for T cells and macrophages

	CD3	CD4	CD8	FoxP3	CD68	CD163
n, samples	54	58	61	60	60	60
n, patients	10	10	10	10	10	10
Peritumoral clustering, *n* (%)	37 (68.5)	37 (63.8)	35 (57.4)	26 (43.3)	–	–
Intratumoral clustering, *n* (%)	33 (61.1)	40 (69.0)	16 (26.2)	4 (6.7)	–	–
Neither peri- nor intratumoral clustering, *n* (%)	8 (14.8)	6 (10.3)	16 (26.2)	31 (51.7)	–	–
Density of positive cells/mm^2, mean (SD)	397 (435)	–[a]	190 (234)	24 (33)	375 (184)	705 (249)
Density of positive cells/mm^2, median (range)	171 (20-1870)	–[a]	87 (4-1254)	7 (1-121)	378 (5-774)	689 (119-1253)

[a] The density of cells positive for CD4 could not be counted due to the dense mass of positive cells.

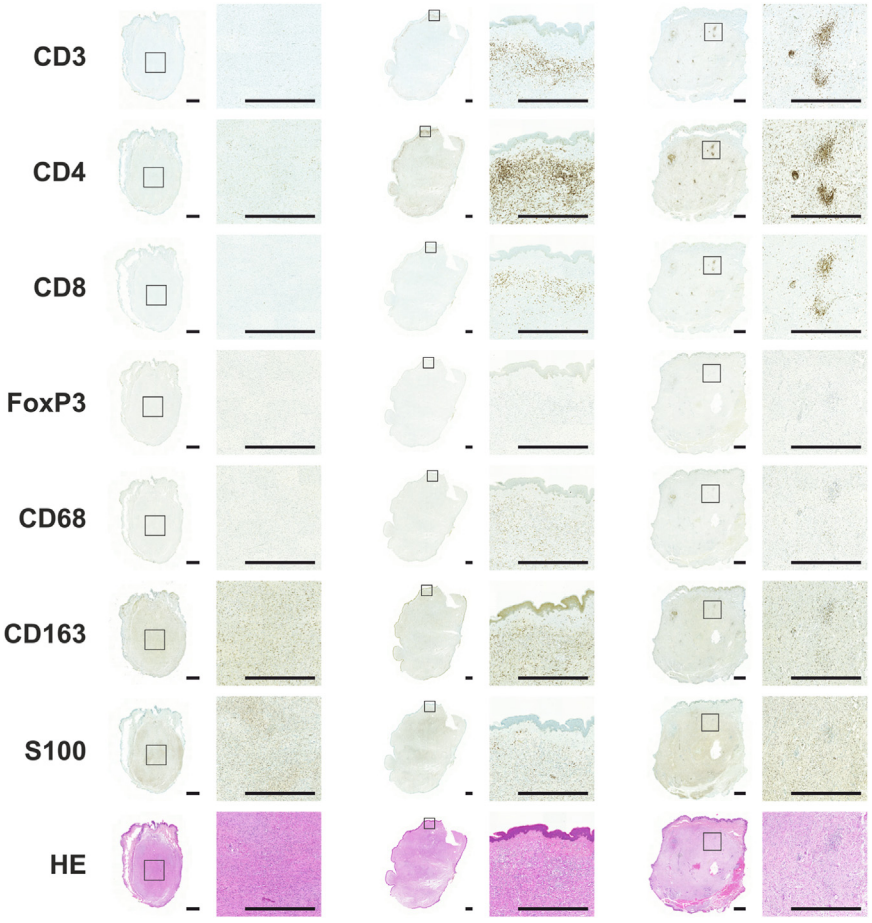

Figure 1.
Representative examples of immune cell distribution in cutaneous neurofibromas. The first 2 columns show an example of a relatively uniform distribution of T cells. The middle columns represent T cell clustering at the epidermal tumor border, and the last 2 columns show intratumoral clusters. The black squares delineate the area shown in greater magnification. Scale bars 1 mm.

somewhat across markers (Table 1). However, the pattern observed for CD3-positive cells generally corresponded to the patterns seen in CD4- and CD8-positive cells. When compared with HE staining and S100 immunolabeling, it was evident that the immune cells located at the tumor border were predominantly within the tumor instead of the surrounding dermis. Among the tumors with clustering of CD3-positive cells at the tumor border, the clustering was nearly always located in the area directly under epidermis (97% of cNFs) and only rarely at other borders of the tumor (5.4% of cNFs).

The peritumoral clustering of CD3-positive cells was observed in 88% of cNFs from individuals with a total of >500 cNFs and in 48% of cNFs from individuals with fewer than 500 tumors ($P = .016$; Supplementary Table S2). The difference was statistically significant also in the case of CD4-positive cells ($P = .045$) and borderline nonsignificant for CD8-positive cells ($P = .077$). Tumors with cellularity above the data set median of 3486 cells/mm^2 had fewer intratumoral clusters of CD4-positive cells (50%) compared with the cNFs with cellularity below the data set median (87%; $P = .033$). The proportion of cNFs with intratumoral clusters of cells positive for CD4 was also borderline significantly higher in large tumors (87%) compared with smaller tumors (50%; $P = .046$). The presumed growth status of the tumor, tumor location, or patient age at tumor excision showed no statistically significant association with the spatial distribution of T cells (Supplementary Table S2).

Cells positive for CD4 were clearly more abundant than cells positive for CD3, CD8, or FoxP3 (Fig. 1). The cells positive for CD4 were too densely packed to allow reliable quantification of the cell number, and a subpopulation of CD4-positive cells showed morphology consistent with that of macrophages. Thus, we decided to quantify the densities of CD3-, CD8-, and FoxP3-positive cells only (Table 1). We observed an average of 397 CD3-positive cells/mm^2, corresponding to an average of 9.3% (SD, 9.2; 0.61%-40%) of all the cells in cNFs. The average densities of cells positive for CD8 and FoxP3 were 190 and 24 cells/mm^2, respectively. The CD8-positive cells represented an average of 5.0% (SD, 5.4; 0.21%-27%), and cells positive for FoxP3 represented an average of 0.55% (SD, 0.69; 0.018%-2.5%) of all the cells in cNFs. The density of CD8-positive cells was, on average, 34% (SD, 14; 4.7%-61%) of the density of CD3-positive cells, and the density of FoxP3-positive cells was 5.5% (SD, 5.2; 1.0%-31%) of the density of CD3-positive cells. The densities of positive cells were generally higher in the samples with peritumoral clustering of positive cells.

Tumors from individuals younger than the median age of participants (33 years) harbored higher densities of cells positive for CD3, CD8, or FoxP3 than tumors from older individuals (Fig. 2). In addition, growing tumors and tumors smaller than the data set median of 8.7 mm^2 showed increased T cell density. The T cell density showed no significant associations with patient sex, tumor location, patient's total number of cNFs, or tumor cellularity. A similar pattern of associations with clinical characteristics was

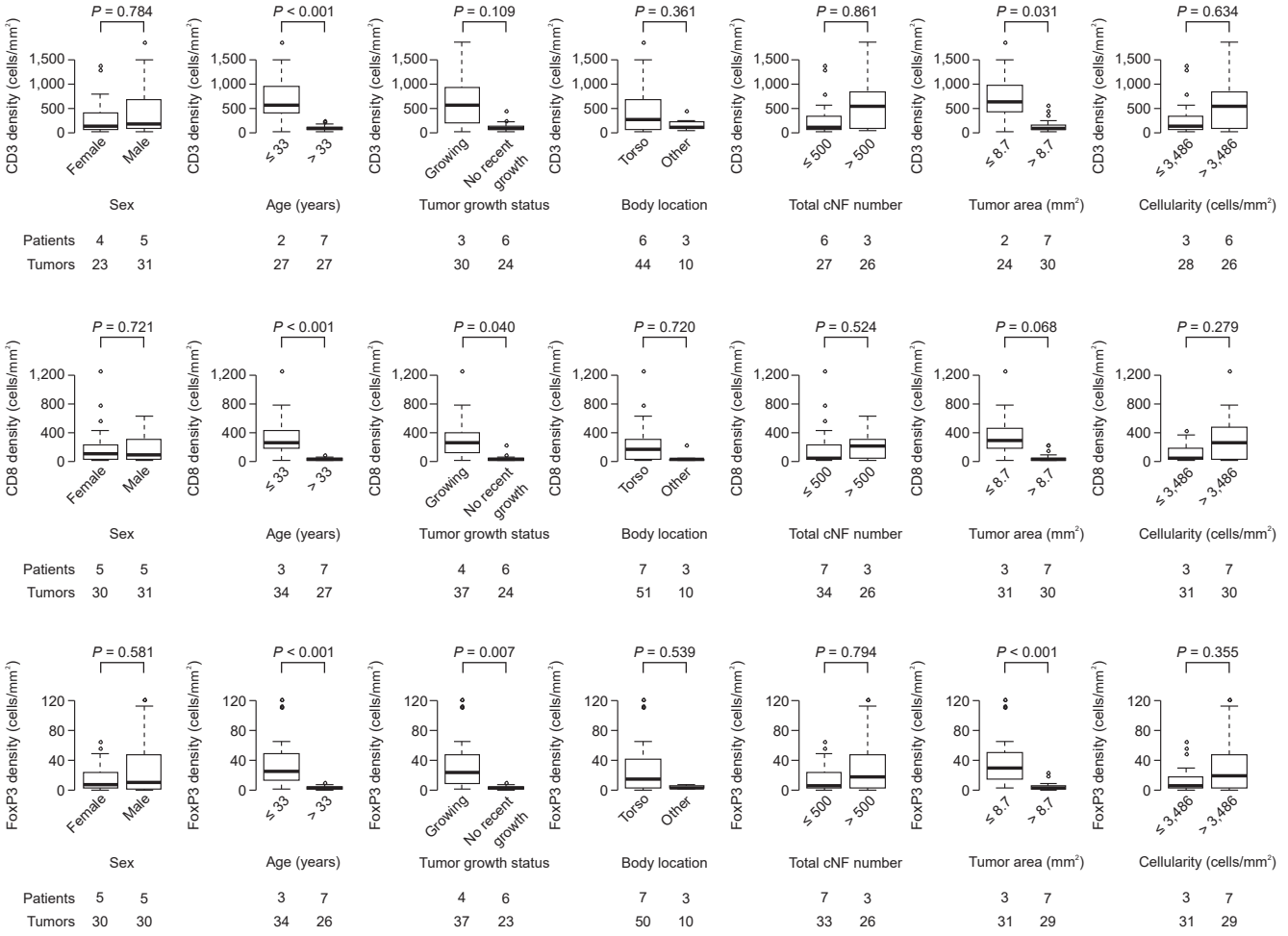

Figure 2.
The associations of clinical and tumor characteristics with the densities of cells positive for CD3, CD8, or FoxP3.

observed in our previous study on mast cells in cNFs.[16] The density of cells positive for the mast cell marker CD117[16] was, indeed, positively correlated with the density of cells positive for CD3 ($P < .001$), CD8 ($P < .001$), and FoxP3 ($P < .001$). The ratio of CD3-positive cells to CD8-positive cells ranged from 1.6 to 21 (mean 3.9, median 3.0) and was smaller in tumors from individuals with more than 500 cNFs ($P = .032$).

To further characterize the immune cell populations in cNFs, we performed immunofluorescence labeling of cells positive for both CD25 and FoxP3. The double-positive cells were few, yet present in cNFs (Supplementary Fig. S1). We also observed scattered IL-25-positive cells and CTLA4-positive cells (Supplementary Fig. S1).

Immunolabeling of Macrophages in Cutaneous Neurofibromas

Cells positive for the macrophage markers CD68 and CD163 were abundant in cNFs. The mean density of CD163-positive cells, 705 cells/mm^2, was clearly higher than the density of 397 CD3-positive cells/mm^2 (Table 1). CD68 positivity was also common in cNFs with a mean density of 375 cells/mm^2. The density of cells positive for CD68 or CD163 was not associated with the presence of peritumoral clusters of cells positive for CD3 or CD4, yet the intratumoral clusters of CD3-positive cells were associated with increased densities of cells positive for CD68 ($P = .062$) and CD163 ($P = .011$). The density of cells positive for CD68 or CD163 seemed to be negatively associated with the density of cells positive for the T cell marker CD3 ($P = .044$ and $P = .026$, respectively), yet the result was largely influenced by high T cell densities in the tumors of 2 patients (Supplementary Fig. S2). Interestingly, tumors with a relatively low density of CD3-positive cells could harbor various densities of CD68- and CD163-positive cells. The mast cell marker CD117 also showed a negative correlation with the density of cells positive for CD68 or CD163 ($P < .001$ and $P = .016$, respectively), yet the variation was large (Supplementary Fig. S2).

Larger tumors had a higher density of cells positive for CD68 ($P = .041$), but such an association was not observed in the case of CD163-positive cells ($P = .331$; Fig. 3). The density of cells positive for CD163 was significantly lower in the tumors from individuals with >500 cNFs compared with cNFs from individuals with fewer tumors ($P = .007$). The density of cells positive for CD68 or CD163 was not associated with patient sex or age or tumor growth status, location, or cellularity (Fig. 3).

Mass Spectrometry Analysis of Immunologic Processes in Cutaneous Neurofibromas

The mass spectrometric analysis of tissue protein content enabled a comparison of 15 cNFs with their overlying skin.

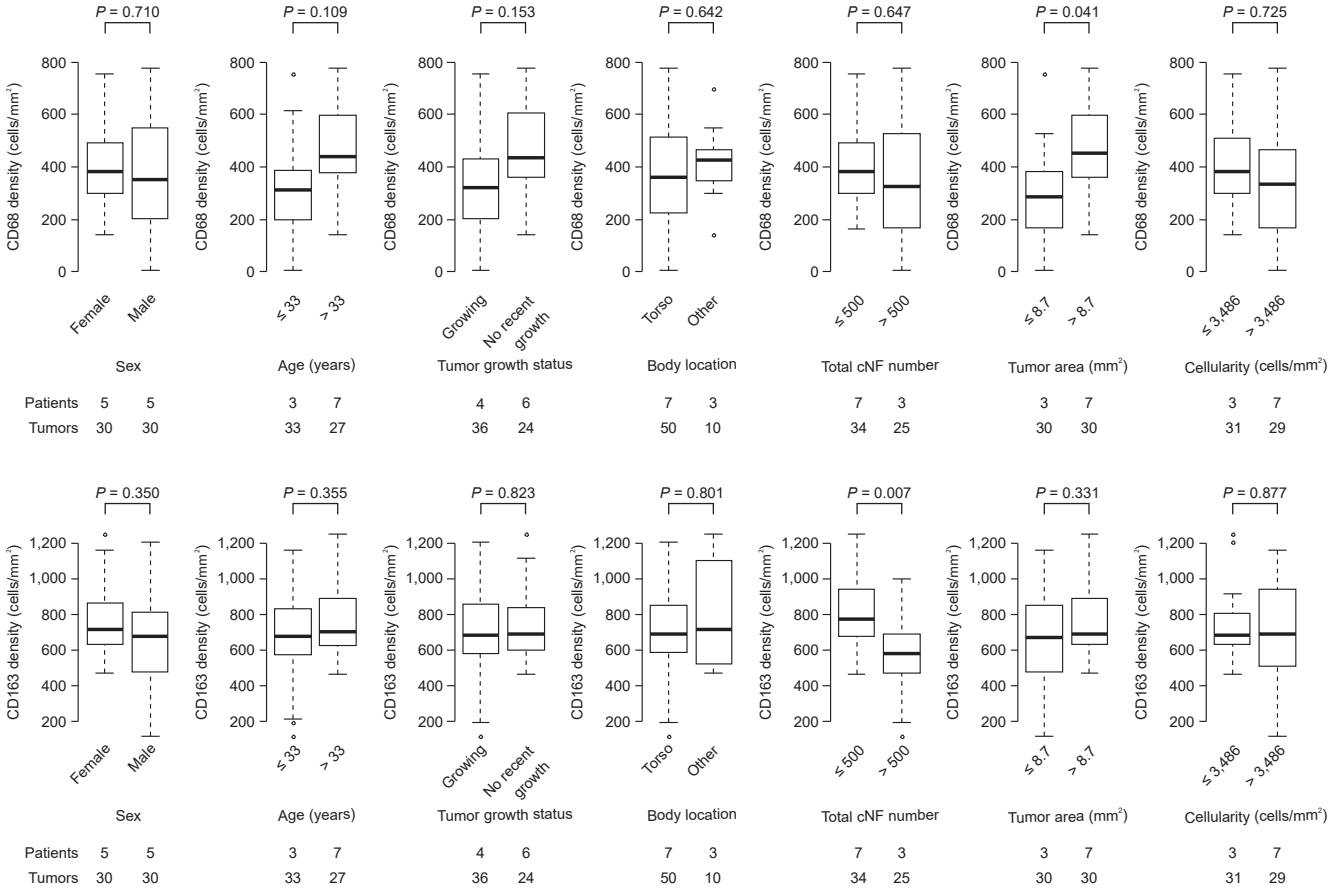

Figure 3.
The associations of clinical and tumor characteristics with the densities of cells positive for CD68 or CD163.

Although numerous immune-related GO-terms scored comparably for both cNFs and skin, several differences were noted (Table 2; Supplementary Table S3). The cNFs showed significant increases in processes related to complement activation, B cell activation, and immunoglobulins. For example, proteins associated with complement activation displayed a 14% (95% CI, 9%-20%) increase, and proteins associated with the B cell receptor signaling pathway showed a 16% (95% CI, 8%-25%) increase in cNFs compared with the skin. On the contrary, processes related to T cell-mediated immunity were decreased in cNFs compared with the skin (Table 2).

When individual proteins were examined in the MS data, the anti-inflammatory proteins associated with regulatory T cells, CD39 and CD73, showed 53% (95% CI, 11%-76%; $P = .145$) and 38% (95% CI, 19%-52%; $P = .013$), respectively, decreases in expression in cNFs compared with skin. The transcription factor STAT6 involved in the differentiation of T-helper type 2 cells also showed lower levels in cNFs compared with skin (0.65, 95% CI, 0.52-0.81; $P = .009$). The monocyte/macrophage marker CD14 was higher by 59% (95% CI, 18%-114%; $P = .028$) in cNFs compared with skin; however, the expression of CD163 showed no difference between the 2 tissue types (0.94; 95% CI, 0.67-1.32; $P = 1.000$).

Characterization of Tumor T Cell Population by T Cell Receptor Sequencing

The analysis of 8 cNFs from 3 patients with NF1 revealed an average of 1473 (SD, 599) TCR rearrangements per cNF. These yielded an average of 2885 (SD, 1956) templates per cNF, reflecting the number of T cells in the samples. The mean numbers of TCR rearrangements were significantly higher in the skin (6428; SD, 3048) and blood (28,807; SD, 10,472) than in cNFs ($P < .001$ in both comparisons). An average of 80.6% (SD, 7.1) of templates was productive in cNFs, whereas the respective proportions were 81.5% (SD, 6.1) in the skin and 83.7% (SD, 4.3) in the blood. The average productive Simpson clonality was 0.062 (SD, 0.012) in cNFs. The mean values of productive Simpson clonality of 0.070 (SD, 0.018) in skin and 0.092 (SD, 0.103) in blood did not significantly differ from that of cNFs ($P = .185$ and $P = .174$, respectively).

Morisita's overlap index showed negligible overlap of rearrangements between samples from different patients with values ranging from 0 to 0.005. The overlap of rearrangements between the different cNFs of a patient was similar to the overlap between the skin samples of a patient ($P = .192$) or to the overlap between cNFs and skin ($P = .654$; Fig. 4A). Interestingly, the mean Morisita index was 0.139 between cNFs and blood and 0.049 between skin and blood ($P = .003$), suggesting greater involvement of blood T cells in cNFs than in skin. The tumor and skin samples of patient 3 showed exceptionally high values of the Morisita index (Fig. 4A). Patient 3 also showed the highest maximum productive frequency of 20% of a single rearrangement.

To further examine productive rearrangements shared by different cNFs, we excluded the rearrangements present in the blood, since blood may have cross-contaminated the cNF and skin samples during tumor excision. Only a few productive

Table 2
The immune-related GO terms differing significantly between cutaneous neurofibromas and overlying skin after Bonferroni correction

GO term	Proteins	Estimate (95% CI)	Corrected *P* value
Antigen processing and presentation of peptide or polysaccharide antigen via MHC class II (GO:0002504))	7	0.22 (0.14-0.36)	<.001
Inflammatory response to antigenic stimulus (GO:0002437))	5	0.25 (0.14-0.45)	.001
MHC class II protein complex (GO:0042613))	9	0.27 (0.19-0.40)	<.001
Negative regulation of T cell proliferation (GO:0042130))	5	0.36 (0.29-0.45)	<.001
B cell differentiation (GO:0030183))	6	0.37 (0.21-0.65)	.047
Peptide antigen binding (GO:0042605)	6	0.49 (0.43-0.57)	<.001
Negative regulation of interferon-gamma production (GO:0032689)	7	0.52 (0.43-0.62)	<.001
Antimicrobial humoral immune response mediated by antimicrobial peptide (GO:0061844)	19	0.52 (0.41-0.67)	<.001
Negative regulation of activated T cell proliferation (GO:0046007)	5	0.55 (0.44-0.70)	<.001
Antigen processing and presentation of endogenous peptide antigen via MHC class I (GO:0019885)	5	0.59 (0.48-0.73)	<.001
Cellular response to interleukin-4 (GO:0071353)	10	0.60 (0.53-0.68)	<.001
Positive regulation of T cell mediated cytotoxicity (GO:0001916)	7	0.62 (0.54-0.71)	<.001
Negative regulation of inflammatory response (GO:0050728)	11	0.65 (0.57-0.74)	<.001
Positive regulation of interleukin-8 production (GO:0032757)	15	0.66 (0.53-0.83)	.029
Positive regulation of T cell activation (GO:0050870)	6	0.67 (0.59-0.76)	<.001
Adaptive immune response (GO:0002250)	36	0.68 (0.60-0.77)	<.001
T cell activation (GO:0042110)	9	0.69 (0.60-0.79)	<.001
Inflammatory response (GO:0006954)	54	0.69 (0.62-0.78)	<.001
Cellular response to interleukin-7 (GO:0098761)	8	0.70 (0.63-0.76)	<.001
Leukocyte cell-cell adhesion (GO:0007159)	14	0.70 (0.62-0.78)	<.001
T cell differentiation in thymus (GO:0033077)	6	0.71 (0.62-0.82)	<.001
Negative regulation of cytokine production involved in inflammatory response (GO:1900016)	5	0.72 (0.60-0.85)	.017
Complement component C1q complex binding (GO:0001849)	5	0.72 (0.61-0.85)	.014
Cellular response to interferon-gamma (GO:0071346)	25	0.73 (0.64-0.83)	<.001
Interleukin-12-mediated signaling pathway (GO:0035722)	32	0.75 (0.70-0.80)	<.001
Antigen processing and presentation (GO:0019882)	17	0.75 (0.67-0.83)	<.001
Positive regulation of interleukin-10 production (GO:0032733)	8	0.75 (0.66-0.86)	.002
Interleukin-1-mediated signaling pathway (GO:0070498)	47	0.75 (0.69-0.81)	<.001
Negative regulation of T cell receptor signaling pathway (GO:0050860)	6	0.75 (0.67-0.84)	<.001
Interferon-gamma-mediated signaling pathway (GO:0060333)	15	0.76 (0.70-0.83)	<.001
Regulation of immune response (GO:0050776)	48	0.77 (0.69-0.86)	<.001
Activation of innate immune response (GO:0002218)	11	0.77 (0.69-0.86)	<.001
Cellular response to interferon-beta (GO:0035458)	5	0.78 (0.69-0.90)	.047
MHC class II protein complex binding (GO:0023026)	11	0.79 (0.72-0.86)	<.001
Immunologic synapse (GO:0001772)	15	0.79 (0.72-0.86)	<.001
T cell receptor signaling pathway (GO:0050852)	56	0.80 (0.76-0.84)	<.001
Antigen processing and presentation of exogenous peptide antigen via MHC class I, TAP-dependent (GO:0002479)	50	0.80 (0.75-0.85)	<.001
Antigen processing and presentation of exogenous peptide antigen via MHC class II (GO:0019886)	39	0.81 (0.74-0.89)	.002
Leukocyte migration (GO:0050900)	79	0.86 (0.79-0.94)	.035
Innate immune response (GO:0045087)	120	0.88 (0.83-0.93)	<.001
Regulation of complement activation (GO:0030449)	72	1.12 (1.07-1.17)	<.001
Complement activation, classical pathway (GO:0006958)	84	1.12 (1.07-1.18)	<.001
Complement activation (GO:0006956)	56	1.14 (1.09-1.20)	<.001
Negative regulation of inflammatory response to antigenic stimulus (GO:0002862)	47	1.15 (1.09-1.22)	<.001
B cell receptor signaling pathway (GO:0050853)	39	1.16 (1.08-1.25)	.004
Antigen binding (GO:0003823)	60	1.17 (1.10-1.23)	<.001
Immunoglobulin complex, circulating (GO:0042571)	36	1.19 (1.11-1.28)	<.001
Immunoglobulin receptor binding (GO:0034987)	35	1.19 (1.10-1.29)	.001
Positive regulation of B cell activation (GO:0050871)	37	1.20 (1.11-1.29)	<.001
Immunoglobulin complex (GO:0019814)	28	1.20 (1.10-1.31)	.005

All the analyzed GO terms and uncorrected *P* values are shown in Supplementary Table S3.
GO, gene ontology.

rearrangements were shared by the different tumors of a patient, and none of these were present in all the tumors from different patients (Fig. 4B, C). Most rearrangements shared by different tumors of a patient were also present in the skin (Fig. 4D). To conclude, the results show that skin and cNF host clearly different T cell populations. Each cNF has a unique T cell population, whereas the diversity of tumor T cell population does not differ from that of skin, suggesting that cNFs do not contain dominant tumor-specific T cell clones.

Discussion

Immune cell infiltrates other than mast cells are not usually mentioned in the context of cNFs. However, our current results reveal abundant T-lymphocyte and macrophage infiltration in human cNFs. Correlation of T cell densities with the clinical data indicated that tumors from individuals younger than the median age of study participants (33 years) harbored higher densities of cells positive for CD3, CD8, or FoxP3 than tumors from individuals

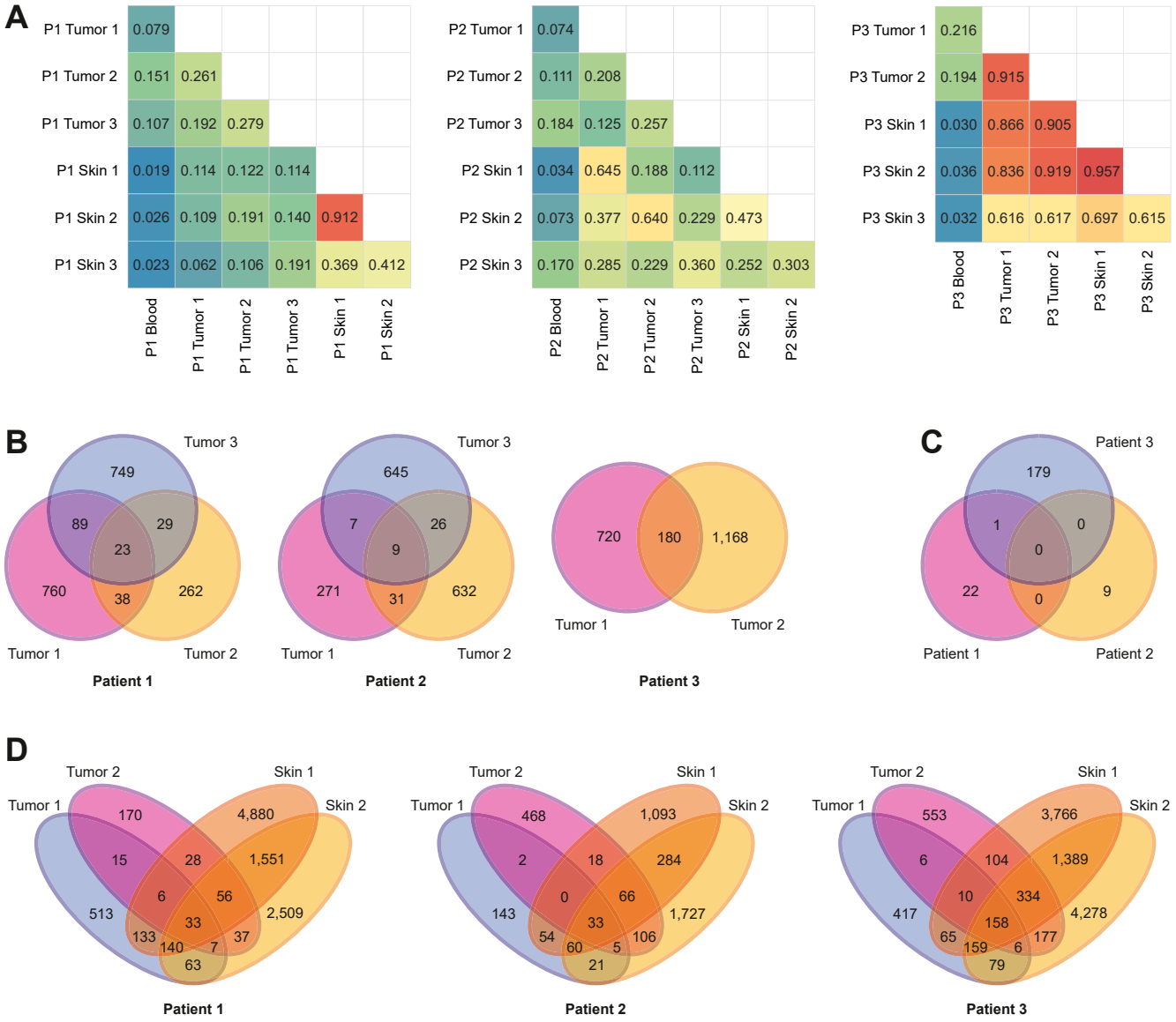

Figure 4.
The overlap of T cell receptor rearrangements between different samples. (A) The values of Morisita's overlap index between the different samples of each patient (P1 to P3). Red shading represents high-index values, and blue shading indicates low values. (B) Productive rearrangements shared between different cutaneous neurofibromas of each patient with NF1 after excluding the rearrangements present in the blood. (C) Overlap between the productive rearrangements present in all cutaneous neurofibromas of a patient after the exclusion of the rearrangements present in the blood. (D) Productive rearrangements shared between cutaneous neurofibromas and the overlying skin in each patient with NF1 after the exclusion of the rearrangements present in the blood.

older than 33 years. Higher T cell densities may also be related to the growth phase of the cNFs since growing tumors and tumors smaller than the median size in the data set showed increased T cell density. We observed no statistically significant associations between T cell density and patient sex, tumor location, patient's total number of cNFs, or tumor cellularity.

The proportion of T cells of all tumor cells varied widely between tumors, ranging from as low as 0.61% to as high as 40%. This is consistent with the marked between-tumor variation of cNFs previously described in terms of, for example, the number of mast cells,[16] PD-L1 expression,[31] or expression of hormone receptors.[49,50] Malignant tumors can be considered immunologically "hot" or "cold" based on the numbers of T cells or their tumor antigens. The results of the present study indicate that some cNFs are immunologically "cold" with minimal T-cell presence, whereas others have a notably high T cell count, potentially representing "hot" tumors. The relative numbers of cytotoxic T cells (CD8-positive) also showed a wide variation between the tumors with an average proportion of 5% of all tumor cells. However, the total number of immune cells in the tumor may not be critical since it has been shown that only a small fraction, maybe 10% of $CD8^+$ cells, can recognize tumor antigens.[51]

Cells positive for CD3, CD4, CD8, and FoxP3 were detected in the following 3 patterns of distribution: uniformly scattered throughout the tumor, clustered inside the tumor, and clustered in the tumor border facing the dermis of the overlying skin. These patterns were partly overlapping. The clustering of T cells was consistent with a previous study that described patchy distribution of cells positive for CD3 and CD8 in cNFs.[31] These observations highlight the intratumor heterogeneity in immune cell

populations within cNFs, despite the relatively uniform distribution of Schwann cells and the collagenous matrix. Future research should consider this within-tumor variation especially when using tissue microarrays or analyzing dissociated cells and tumor lysates.

The patterns of the spatial distribution of immune cells in cNFs show a potential analogy with those described in malignant tumors: inflamed tumors display the scattering of immune cells between the cancer cells and respond well to immunotherapy, whereas immune-excluded cancers show the restriction of the immune infiltration to tumor border and rarely respond to immune therapy.[52] We observed that individuals with more than 500 cNFs had an increased rate of peritumoral clustering of CD3- and CD4-positive cells. However, the patterns of T cell distribution showed no statistically significant association with the presumed growth status of the tumor, tumor location, or patient age. These findings could suggest some host-related characteristics leading to the accumulation of immune cells at the peritumoral region instead of the inner parts of the tumor, thereby allowing the development of a large number of cNFs. On one hand, T cell infiltrates in the tumor borders may restrict tumor growth since peritumoral $CD8^+$ cells have been correlated with favorable prognosis in hepatocellular cancer.[53] On the other hand, peritumoral infiltrates may inhibit the contact of effector T cells with tumor cells.[54] The significance of peritumoral T cells in cNFs remains to be elucidated.

Mutations can produce neoepitopes expressed on transformed cells.[55] Tumor-initiating Schwann cells in cNFs have double mutations in the *NF1* tumor-suppressor gene ($NF1^{-/-}$ Schwann cells), and the somatic second hit varies between the cNFs.[11,12,56] $NF1^{-/-}$ Schwann cells could be speculated to express *NF1*-related neoepitopes that could be immunogenic, yet they are not eradicated by the immune system. High mutational burden is associated with increased tumor immunogenicity,[52] and somatic mutations other than the *NF1* second-hit are infrequent in cNFs.[57] The lack of immunogenic neoepitopes, poor access of immune cells into the tumor, or an immune suppressive microenvironment may underlie the lack of immune eradication of mutant Schwann cells in cNFs. The previous reports of PD-L1 expression in cNFs could speak in favor of immune suppression.[30,31] Regulatory T cells are essential in maintaining tolerance to self/autoantigens,[58,59] and they can also be permissive to tumor growth.[18] A subpopulation of the FoxP3-positive cells observed in the present study also expressed CD25, suggesting that these were regulatory T cells, although we did not formally verify the presence of $CD4^+CD25^+$ cells nor compute the ratio of cells positive for FoxP3 and CD4. Cells positive for FoxP3 have also previously been described in neurofibromas, with slightly smaller density in diffuse dermal neurofibromas than in diffuse neurofibromas located elsewhere.[30] Intratumoral regulatory T cells in cNFs could be speculated to inhibit the eradication of $NF1^{-/-}$ Schwann cells and thus to be permissive or even favor tumor growth. The presence of $FoxP3^+$ cells, albeit at a relatively low density, and the abundance of cells positive for the general T cell and macrophage markers suggest that cNFs might potentially be amenable to immune therapies.

We have previously studied mast cells in the same tumor material as analyzed in the current study[16] and found that the density of mast cells correlates with the patient age, tumor size, and growth status, as described here for T cells. In fact, we observed positive correlations between the density of mast cells and the densities of CD3-, CD8-, and FoxP3-positive T cells. This suggests that high densities of both mast cells and T cells may be present in the small and still-growing cNFs of young individuals.

The current study shows that the number of cells positive for CD4 exceeded the number of cells positive for CD3, suggesting that the CD4 population contains also other cell types in addition to T cells. Since also macrophages can be CD4-positive, we used macrophage markers CD68 and CD163 and visualized abundant macrophage populations in cNFs. CD68 is usually considered a pan-macrophage marker, whereas CD163 can be considered a marker for M2 macrophages. In the present study, the density of cells positive for CD163 was higher than the density of cells positive for CD68, and we do not have an explanation for this observation. However, the $CD163^+$ and $CD68^+$ cells have been reported to constitute distinct macrophage populations in melanoma,[60] and the presence of $CD68^-$ $CD163^+$ cells has also been described in, for example, breast cancer.[61]

The high density of cells positive for CD163 is in contrast to a study that reported only a few cells positive for CD163 in plexiform neurofibromas.[25] The density of macrophages was lower in cNFs from individuals who had over 500 tumors while it was not associated with age, sex, tumor growth status, location, or cellularity. Tumor-associated M2 macrophages are considered tumor-permissive since they can promote tumor growth by releasing growth factors and cytokines that stimulate the proliferation of tumor cells, they can suppress anti-tumor immunity, or they may contribute to tumor growth by promoting angiogenesis.[62] A previous study on a genetically engineered mouse model has shown that macrophages are abundant in mouse neurofibromas and that inactivation of *Nf1* in Schwann cells leads to the recruitment of macrophages in peripheral nerves.[25] It can be speculated that there is an interplay between Schwann cells and macrophages also in human cNFs, but the present study cannot verify a permissive role of macrophages in cNFs.

The density of immune cells showed considerable variation both within and across individuals (Supplementary Fig. S2). The varying numbers of cNFs per patient included in the study were taken into account by using a patient-specific random intercept in the statistical analyses. However, many of the clinical variables, such as patient age, tumor size, and tumor growth status, are highly intercorrelated. Future studies need to elucidate these interconnections, for example, by restricting the analysis to a specific age group. A minor proportion of the sample slides was damaged during the processing, leading to slight discrepancies in the number of tumors labeled for each marker (Table 1). Nevertheless, the labeling of the same tumors for multiple markers allows a more reliable understanding of the connections between immune cell types than studying different markers in unrelated tumors.

Mass spectrometry analysis was carried out to study immunologic processes in cNFs. The skin overlying the tumors was used as a point of comparison. The results showed that the skin is clearly different from the tumor, which should be considered when planning studies on whole tumor samples also containing the skin. Skin is the primary interface between the tissues and the environment, and resident T cells in the dermis are crucial for immune responses against pathogenic micro-organisms. Thus, it was not surprising that immunologic processes related to T cell-mediated immunity were decreased in cNFs compared with the skin, and the number of TCR rearrangements was lower in cNFs than in the skin. Protein expression associated with complement activation was increased in cNFs compared with skin. This is interesting because complement has gained increasing attention in the context of tumorigenesis and cancer during the past 5 to 10

years. For example, in the skin, the role of the classical pathway and several inhibitors have been shown in the regulation of progression of cutaneous squamous cell carcinoma,[63-66] and complement is being studied to find potential biomarkers and treatment targets for tumor immunotherapy.[65,67]

Sequencing of the CDR3 region of TCR was carried out to further analyze the T cell population of the tumors. Although the skin covering the tumor and the tumor itself contained partly shared T cell populations, each cNF also had a unique T cell population. T cells with specificity for the tumor structures may therefore exist, yet no dominant cNF-related clones were observed. It is possible that most of the immune cells in cNFs are just innocent bystanders, yet it is of interest what has attracted the cells to the tumor and what their function is.

We believe that the results of this study can be used as a general resource on the immune cell content of human cNFs. The results should be seen as an overview of the immune microenvironment of cNFs partly filling the knowledge gap in the tumor microenvironment of cNFs, and the results lead to numerous more detailed questions. Understanding the immunology of malignant tumors is essential for cancer treatments, yet understanding the mechanisms of immune escape particularly in benign tumors is important for elucidating more general mechanisms of tumor growth. In addition to being useful in the context of cNFs, this study could also add knowledge more generally on tumor microenvironment of benign tumors and other heritable cancer syndromes.

Acknowledgments

Mass spectrometry analyses were performed at the Turku Proteomics Facility supported by Biocenter Finland. Immunohistochemistry services were obtained from the Histology core facility of the Institute of Biomedicine, University of Turku, Finland, and the Pathology Laboratory of Turku University Hospital, Turku, Finland. This study has been carried out in Turku University Hospital, which is a member of the European Reference Network on Genetic Tumour Risk Syndromes (ERN GENTURIS). ERN GENTURIS is funded by the European Union.

Author Contributions

R.A.K., S.P., E.M., M.S., I.L., and J.P. conceptualized the study. R.A.K., S.P., K.L., E.M., M.J., P.R., and J.P. collected the samples and curated the data. R.A.K., S.P., K.L., E.M., M.J., E.F., I.L., and J.P. designed and performed the image analyses. P.H. and A.R. performed the mass spectrometry measurements. R.A.K. performed the statistical analyses. R.A.K., S.P., and J.P. acquired funding for the study. S.P. and J.P. supervised the study. R.A.K., S.P., and J.P. wrote the initial draft of the manuscript. All authors participated in the interpretation of the results, reviewed and edited the manuscript, and approved the final version of the manuscript.

Data Availability

Immunohistochemistry data for CD3, CD4, CD8, FoxP3, CD68, and CD163 expressions in cNFs are available at https://doi.org/10.7303/syn51314057. The previously reported[16] data set of immunolabeling for the mast cell marker CD117 is available at https://doi.org/10.7303/syn25613686. The T cell receptor sequencing data set is available at https://doi.org/10.7303/syn51315874.

Funding

This publication was supported by a Subagreement from the Johns Hopkins University via the Neurofibromatosis Therapeutic Acceleration Program (NTAP) with funds provided by Grant Agreement form the Bloomberg Family Foundation. Its contents are solely the responsibility of the authors and do not necessarily represent the official views of the Bloomberg Family Foundation or the Johns Hopkins University.

Declaration of Competing Interest

The authors declare no conflicts of interest.

Ethics Approval and Consent to Participate

The study adhered to the principles of the Declaration of Helsinki and was approved by the Ethics Committee of the Hospital District of Southwest Finland, and Turku University Hospital. All participants provided their written informed consent.

Supplementary Material

The online version contains supplementary material available at https://doi.org/10.1016/j.labinv.2023.100285

References

1. DeBella K, Szudek J, Friedman JM. Use of the national institutes of health criteria for diagnosis of neurofibromatosis 1 in children. *Pediatrics*. 2000;105(3 Pt 1):608–614. https://doi.org/10.1542/peds.105.3.608
2. Ferner RE, Huson SM, Thomas N, et al. Guidelines for the diagnosis and management of individuals with neurofibromatosis 1. *J Med Genet*. 2007;44(2):81–88. https://doi.org/10.1136/jmg.2006.045906
3. Gutmann DH, Ferner RE, Listernick RH, Korf BR, Wolters PL, Johnson KJ. Neurofibromatosis type 1. *Nat Rev Dis Prim*. 2017;3:17004. https://doi.org/10.1038/nrdp.2017.4
4. Kodra Y, Giustini S, Divona L, et al. Health-related quality of life in patients with neurofibromatosis type 1: a survey of 129 Italian patients. *Dermatology*. 2009;218(3):215–220. https://doi.org/10.1159/000187594
5. Guiraud M, Bouroubi A, Beauchamp R, et al. Cutaneous neurofibromas: patients' medical burden, current management and therapeutic expectations: results from an online European patient community survey. *Orphanet J Rare Dis*. 2019;14(1):286. https://doi.org/10.1186/s13023-019-1265-4
6. Wallace MR, Marchuk DA, Andersen LB, et al. Type 1 neurofibromatosis gene: Identification of a large transcript disrupted in three NF1 patients. *Science*. 1990;249(4965):181–186. https://doi.org/10.1126/science.2134734
7. Xu G, O'Connell P, Viskochil D, et al. The neurofibromatosis type 1 gene encodes a protein related to GAP. *Cell*. 1990;62(3):599–608. https://doi.org/10.1016/0092-8674(90)90024-9
8. Kallionpää RA, Uusitalo E, Leppävirta J, Pöyhönen M, Peltonen S, Peltonen J. Prevalence of neurofibromatosis type 1 in the Finnish population. *Genet Med*. 2018;20(9):1082–1086. https://doi.org/10.1038/gim.2017.215
9. Uusitalo E, Rantanen M, Kallionpää RA, et al. Distinctive Cancer Associations in Patients With Neurofibromatosis Type 1. *J Clin Oncol*. 2016;34(17):1978–1986. https://doi.org/10.1200/JCO.2015.65.3576
10. Evans DGR, Baser ME, McGaughran J, Sharif S, Howard E, Moran A. Malignant peripheral nerve sheath tumours in neurofibromatosis 1. *J Med Genet*. 2002;39(5):311–314. https://doi.org/10.1136/JMG.39.5.311
11. Serra E, Rosenbaum T, Winner U, et al. Schwann cells harbor the somatic NF1 mutation in neurofibromas: evidence of two different Schwann cell subpopulations. *Hum Mol Genet*. 2000;9(20):3055–3064. https://doi.org/10.1093/hmg/9.20.3055
12. Maertens O, Brems H, Vandesompele J, et al. Comprehensive NF1 screening on cultured Schwann cells from neurofibromas. *Hum Mutat*. 2006;27(10):1030–1040. https://doi.org/10.1002/humu.20389
13. Le LQ, Shipman T, Burns DK, Parada LF. Cell of Origin and Microenvironment Contribution for NF1-Associated Dermal Neurofibromas. *Cell Stem Cell*. 2009;4(5):453–463. https://doi.org/10.1016/j.stem.2009.03.017
14. Peltonen J, Jaakkola S, Lebwohl M, et al. Cellular differentiation and expression of matrix genes in type 1 neurofibromatosis. *Lab Invest*. 1988;59(6):760–771.

15. Jouhilahti EM, Peltonen S, Callens T, et al. The development of cutaneous neurofibromas. *Am J Pathol*. 2011;178(2):500–505. https://doi.org/10.1016/j.ajpath.2010.10.041
16. Kallionpää RA, Ahramo K, Martikkala E, et al. Mast cells in human cutaneous neurofibromas: density, subtypes, and association with clinical features in neurofibromatosis 1. *Dermatology*. 2022;238(2):329–339. https://doi.org/10.1159/000517011
17. Belluco S, Sammarco A, Sapin P, Lurier T, Marchal T. FOXP3, CD208, and CD206 expression in canine cutaneous histiocytoma. *Vet Pathol*. 2020;57(5):599–607. https://doi.org/10.1177/0300985820941818
18. Calì B, Molon B, Viola A. Tuning cancer fate: the unremitting role of host immunity. *Open Biol*. 2017;7(4):170006. https://doi.org/10.1098/rsob.170006
19. Hussein MR, Elsers DAH, Fadel SA, Omar AEM. Immunohistological characterisation of tumour infiltrating lymphocytes in melanocytic skin lesions. *J Clin Pathol*. 2006;59(3):316–324. https://doi.org/10.1136/jcp.2005.028860
20. Mourmouras V, Fimiani M, Rubegni P, et al. Evaluation of tumour-infiltrating CD4+CD25+FOXP3+ regulatory T cells in human cutaneous benign and atypical naevi, melanomas and melanoma metastases. *Br J Dermatol*. 2007;157(3):531–539. https://doi.org/10.1111/j.1365-2133.2007.08057.x
21. Liao CP, Booker RC, Brosseau JP, et al. Contributions of inflammation and tumor microenvironment to neurofibroma tumorigenesis. *J Clin Invest*. 2018;128(7):2848–2861. https://doi.org/10.1172/JCI99424
22. Fletcher JS, Springer MG, Choi K, et al. STAT3 inhibition reduces macrophage number and tumor growth in neurofibroma. *Oncogene*. 2019;38(15):2876–2884. https://doi.org/10.1038/s41388-018-0600-x
23. Yang FC, Ingram DA, Chen S, et al. Nf1-dependent tumors require a microenvironment containing Nf1+/– and c-kit-dependent bone marrow. *Cell*. 2008;135(3):437–448. https://doi.org/10.1016/j.cell.2008.08.041
24. Dodd RD, Lee CL, Overton T, et al. NF1+/- hematopoietic cells accelerate malignant peripheral nerve sheath tumor development without altering chemotherapy response. *Cancer Res*. 2017;77(16):4486–4497. https://doi.org/10.1158/0008-5472.CAN-16-2643
25. Prada CE, Jousma E, Rizvi TA, et al. Neurofibroma-associated macrophages play roles in tumor growth and response to pharmacological inhibition. *Acta Neuropathol*. 2013;125(1):159–168. https://doi.org/10.1007/s00401-012-1056-7
26. Choi K, Komurov K, Fletcher JS, et al. An inflammatory gene signature distinguishes neurofibroma Schwann cells and macrophages from cells in the normal peripheral nervous system. *Sci Rep*. 2017;7:43315. https://doi.org/10.1038/srep43315
27. Fletcher JS, Wu J, Jessen WJ, et al. Cxcr3-expressing leukocytes are necessary for neurofibroma formation in mice. *JCI insight*. 2019;4(3). https://doi.org/10.1172/jci.insight.98601
28. Guo X, Pan Y, Xiong M, et al. Midkine activation of CD8+ T cells establishes a neuron-immune-cancer axis responsible for low-grade glioma growth. *Nat Commun*. 2020;11(1):2177. https://doi.org/10.1038/s41467-020-15770-3
29. Brosseau JP, Liao CP, Wang Y, et al. NF1 heterozygosity fosters de novo tumorigenesis but impairs malignant transformation. *Nat Commun*. 2018;9(1):5014. https://doi.org/10.1038/s41467-018-07452-y
30. Haworth KB, Arnold MA, Pierson CR, et al. Immune profiling of NF1-associated tumors reveals histologic subtype distinctions and heterogeneity: implications for immunotherapy. *Oncotarget*. 2017;8(47):82037–82048. https://doi.org/10.18632/oncotarget.18301
31. Wang S, Liechty B, Patel S, et al. Programmed death ligand 1 expression and tumor infiltrating lymphocytes in neurofibromatosis type 1 and 2 associated tumors. *J Neurooncol*. 2018;138(1):183–190. https://doi.org/10.1007/s11060-018-2788-6
32. Shurell E, Singh AS, Crompton JG, et al. Characterizing the immune microenvironment of malignant peripheral nerve sheath tumor by PD-L1 expression and presence of CD8+ tumor infiltrating lymphocytes. *Oncotarget*. 2016;7(39):64300–64308. https://doi.org/10.18632/oncotarget.11734
33. Farschtschi S, Kluwe L, Park SJ, et al. Upregulated immuno-modulator PD-L1 in malignant peripheral nerve sheath tumors provides a potential biomarker and a therapeutic target. *Cancer Immunol Immunother*. 2020;69(7):1307–1313. https://doi.org/10.1007/s00262-020-02548-1
34. Farschtschi S, Park SJ, Sawitzki B, et al. Effector T cell subclasses associate with tumor burden in neurofibromatosis type 1 patients. *Cancer Immunol Immunother*. 2016;65(9):1113–1121. https://doi.org/10.1007/s00262-016-1871-0
35. Banerjee J, Allaway RJ, Taroni JN, et al. Integrative analysis identifies candidate tumor microenvironment and intracellular signaling pathways that define tumor heterogeneity in NF1. *Genes (Basel)*. 2020;11(2). https://doi.org/10.3390/genes11020226
36. Brosseau JP, Pichard DC, Legius EH, et al. The biology of cutaneous neurofibromas: consensus recommendations for setting research priorities. *Neurology*. 2018;91(2):S14–S20. https://doi.org/10.1212/WNL.0000000000005788
37. Frank ML, Lu K, Erdogan C, et al. T-cell receptor repertoire sequencing in the era of cancer immunotherapy. *Clin Cancer Res*. 2023;29(6):994–1008. https://doi.org/10.1158/1078-0432.CCR-22-2469
38. National Institutes of Health Consensus Development Conference. Neurofibromatosis. Conference statement. *Arch Neurol*. 1988;45(5):575–578.
39. Legius E, Messiaen L, Wolkenstein P, et al. Revised diagnostic criteria for neurofibromatosis type 1 and Legius syndrome: an international consensus recommendation. *Genet Med*. 2021;23(8):1506–1513. https://doi.org/10.1038/s41436-021-01170-5
40. Jouhilahti EM, Peltonen S, Peltonen J. Class III beta-tubulin is a component of the mitotic spindle in multiple cell types. *J Histochem Cytochem*. 2008;56(12):1113–1119. https://doi.org/10.1369/jhc.2008.952002
41. Bankhead P, Loughrey MB, Fernández JA, et al. QuPath: open source software for digital pathology image analysis. *Sci Rep*. 2017;7(1):16878. https://doi.org/10.1038/s41598-017-17204-5
42. Ashburner M, Ball CA, Blake JA, et al. Gene ontology: tool for the unification of biology. The gene ontology consortium. *Nat Genet*. 2000;25(1):25–29. https://doi.org/10.1038/75556
43. Gene Ontology Consortium. The gene ontology resource: enriching a GOld mine. *Nucleic Acids Res*. 2021;49(D1):D325–D334. https://doi.org/10.1093/nar/gkaa1113
44. Robins HS, Campregher PV, Srivastava SK, et al. Comprehensive assessment of T-cell receptor beta-chain diversity in alphabeta T cells. *Blood*. 2009;114(19):4099–4107. https://doi.org/10.1182/blood-2009-04-217604
45. Carlson CS, Emerson RO, Sherwood AM, et al. Using synthetic templates to design an unbiased multiplex PCR assay. *Nat Commun*. 2013;4:2680. https://doi.org/10.1038/ncomms3680
46. Robins H, Desmarais C, Matthis J, et al. Ultra-sensitive detection of rare T cell clones. *J Immunol Methods*. 2012;375(1-2):14–19. https://doi.org/10.1016/j.jim.2011.09.001
47. Venturi V, Kedzierska K, Turner SJ, Doherty PC, Davenport MP. Methods for comparing the diversity of samples of the T cell receptor repertoire. *J Immunol Methods*. 2007;321(1-2):182–195. https://doi.org/10.1016/j.jim.2007.01.019
48. Leick M, Gittelman RM, Yusko E, et al. T cell clonal dynamics determined by high-resolution TCR-β sequencing in recipients after allogeneic hematopoietic cell transplantation. *Biol Blood Marrow Transplant*. 2020;26(9):1567–1574. https://doi.org/10.1016/j.bbmt.2020.04.026
49. Overdiek A, Winner U, Mayatepek E, Rosenbaum T. Schwann cells from human neurofibromas show increased proliferation rates under the influence of progesterone. *Pediatr Res*. 2008;64(1):40–43. https://doi.org/10.1203/PDR.0b013e31817445b8
50. Li H, Zhang X, Fishbein L, et al. Analysis of steroid hormone effects on xenografted human NF1 tumor schwann cells. *Cancer Biol Ther*. 2010;10(8):758–764. https://doi.org/10.4161/cbt.10.8.12878
51. Scheper W, Kelderman S, Fanchi LF, et al. Low and variable tumor reactivity of the intratumoral TCR repertoire in human cancers. *Nat Med*. 2019;25(1):89–94. https://doi.org/10.1038/s41591-018-0266-5
52. Chen DS, Mellman I. Elements of cancer immunity and the cancer-immune set point. *Nature*. 2017;541(7637):321–330. https://doi.org/10.1038/nature21349
53. Yusa T, Yamashita YI, Okabe H, et al. Survival impact of immune cells infiltrating peritumoral area of hepatocellular carcinoma. *Cancer Sci*. 2022;113(12):4048–4058. https://doi.org/10.1111/cas.15437
54. Joyce JA, Fearon DT. T cell exclusion, immune privilege, and the tumor microenvironment. *Science*. 2015;348(6230):74–80. https://doi.org/10.1126/science.aaa6204
55. Türeci Ö, Vormehr M, Diken M, Kreiter S, Huber C, Sahin U. Targeting the heterogeneity of cancer with individualized neoepitope vaccines. *Clin Cancer Res*. 2016;22(8):1885–1896. https://doi.org/10.1158/1078-0432.CCR-15-1509
56. Zhu Y, Ghosh P, Charnay P, Burns DK, Parada LF. Neurofibromas in NF1: Schwann cell origin and role of tumor environment. *Science*. 2002;296(5569):920–922. https://doi.org/10.1126/science.1068452
57. Emmerich D, Zemojtel T, Hecht J, et al. Somatic neurofibromatosis type 1 (NF1) inactivation events in cutaneous neurofibromas of a single NF1 patient. *Eur J Hum Genet*. 2015;23(6):870–873. https://doi.org/10.1038/ejhg.2014.210
58. Vinay DS, Ryan EP, Pawelec G, et al. Immune evasion in cancer: mechanistic basis and therapeutic strategies. *Semin Cancer Biol*. 2015;35:S185–S198. https://doi.org/10.1016/j.semcancer.2015.03.004
59. Rosenblum MD, Way SS, Abbas AK. Regulatory T cell memory. *Nat Rev Immunol*. 2016;16(2):90–101. https://doi.org/10.1038/nri.2015.1
60. Tremble LF, McCabe M, Walker SP, et al. Differential association of CD68+ and CD163+ macrophages with macrophage enzymes, whole tumour gene expression and overall survival in advanced melanoma. *Br J Cancer*. 2020;123(10):1553–1561. https://doi.org/10.1038/s41416-020-01037-7
61. Medrek C, Pontén F, Jirström K, Leandersson K. The presence of tumor associated macrophages in tumor stroma as a prognostic marker for breast cancer patients. *BMC Cancer*. 2012;12:306. https://doi.org/10.1186/1471-2407-12-306
62. Qian BZ, Pollard JW. Macrophage diversity enhances tumor progression and metastasis. *Cell*. 2010;141(1):39–51. https://doi.org/10.1016/j.cell.2010.03.014
63. Riihilä PM, Nissinen LM, Ala-Aho R, et al. Complement factor H: a biomarker for progression of cutaneous squamous cell carcinoma. *J Invest Dermatol*. 2014;134(2):498–506. https://doi.org/10.1038/jid.2013.346

64. Riihilä P, Nissinen L, Farshchian M, et al. Complement factor I promotes progression of cutaneous squamous cell carcinoma. *J Invest Dermatol*. 2015;135(2):579–588. https://doi.org/10.1038/jid.2014.376
65. Riihilä P, Nissinen L, Knuutila J, Rahmati Nezhad P, Viiklepp K, Kähäri VM. Complement system in cutaneous squamous cell carcinoma. *Int J Mol Sci*. 2019;20(14). https://doi.org/10.3390/ijms20143550
66. Riihilä P, Viiklepp K, Nissinen L, et al. Tumour-cell-derived complement components C1r and C1s promote growth of cutaneous squamous cell carcinoma. *Br J Dermatol*. 2020;182(3):658–670. https://doi.org/10.1111/bjd.18095
67. Talaat IM, Elemam NM, Saber-Ayad M. Complement System: an Immunotherapy Target in Colorectal Cancer. *Front Immunol*. 2022;13:810993. https://doi.org/10.3389/fimmu.2022.810993